The Astrophysical Journal, 752:37 (8pp), 2012 June 10 doi:10.1088/0004-637X/752/1/37


# EFFECTS OF PERPENDICULAR DIFFUSION ON ENERGETIC PARTICLES ACCELERATED BY THE INTERPLANETARY CORONAL MASS EJECTION SHOCK

Y. Wang[1,2], G. Qin[1], and M. Zhang[3]
[1] State Key Laboratory of Space Weather, Center for Space Science and Applied Research, Chinese Academy of Sciences, Beijing 100190, China; ywang@spaceweather.ac.cn, gqin@spaceweather.ac.cn
[2] College of Earth Sciences, Graduate University of Chinese Academy of Sciences, Beijing 100049, China
[3] Department of Physics and Space Sciences, Florida Institute of Technology, Melbourne, FL 32901, USA; mzhang@fit.edu
*Received 2011 November 1; accepted 2012 April 9; published 2012 May 23*

## ABSTRACT

In this work, based on a numerical solution of the focused transport equation, we obtained the intensity and anisotropy time profiles of solar energetic particles (SEPs) accelerated by an interplanetary shock in the three-dimensional Parker magnetic field. The shock is treated as a moving source of energetic particles with an assumed particle distribution function. We computed the time profiles of particle flux and anisotropy as measured by an observer at 1 AU, equatorial plane, and various longitudes with respect to the shock propagation direction. With perpendicular diffusion, energetic particles can cross magnetic field lines. Particles may be detected before the observer's field line is connected to the shock. After the observer's field line breaks from the shock front, the observer still can see more particles are injected into its field line. Our simulations show that the particle onset time, peak time, peak intensity, decay rate, and duration of SEP event could be significantly influenced by the effect of perpendicular diffusion. The anisotropy with perpendicular diffusion is almost the same as that without perpendicular diffusion, but there is an obvious difference at the moment when the observer's field line begins to be connected to the shock.

*Key words:* Sun: coronal mass ejections (CMEs) – Sun: heliosphere – Sun: magnetic topology – Sun: particle emission

## 1. INTRODUCTION

Solar energetic particle (SEP) events can roughly be divided into two categories: impulsive events and gradual events. The impulsive events, with the characteristics of short duration and low intensity, are produced by solar flares. Gradual events, usually having high intensity and lasting longer, are related to the shocks driven by coronal mass ejections (CMEs). Even though CME shocks cover a large range of solar longitude and latitude, the source of SEPs is not uniformly distributed in the corona. Depending on its angular location, an observer in the interplanetary space may or may not be directly connected to the source by the magnetic field. Simultaneous multi-spacecraft observations by, e.g., *STEREO*, clearly show a huge difference of SEP time profiles at different longitudes (Liu et al. 2011).

Generally, there are two major approaches to modeling SEP shock acceleration: Heras et al. (1992, 1995), Kallenrode & Wibberenz (1997), Lario et al. (1998), Ng et al. (1999), and Kallenrode (2001) injected SEPs at the shock with an assumed injection strength, while a few other studies also include the acceleration of SEPs by CME shocks (Lee 1983, 2005; Gordon et al. 1999; Zank et al. 2000; Li et al. 2003; Rice et al. 2003; Sokolov et al. 2004). In these models, three important effects of acceleration and propagation mechanisms have been involved. The first effect is the acceleration process by the CME-driven shock. Zank et al. (2000) provided an onion shell model based on the first-order Fermi acceleration mechanism. They used a one-dimensional hydrodynamic code to describe the evolution of the CME-driven shock in the Parker model of interplanetary magnetic field (IMF). Wave excitation by streaming energetic particles produced at shock is included in the model, and the diffusion coefficient is calculated from a wave energy equation. However, the model is only applicable to extremely strong shocks, due to the use of the Bohm diffusion coefficient. Their simulation results reveal that the maximum energy can go up to the order of GeV when shock is near the Sun. Rice et al. (2003) extended the Zank et al. (2000) model so that it is applicable to shock waves of arbitrary strengths. The second effect is the scattering by waves generated by the streaming particles. Ng et al. (1999, 2001, 2003) presented a model of particle transport including streaming proton-generated Alfvén waves, in which the shock acceleration is represented by a moving SEP source, and the particle diffusion coefficients are expressed by wave intensity and wave growth rates. Their simulation results agree well with the observed evolution of spectral slope and abundance ratios of heavy ions in gradual SEP events, and they show that the wave amplification plays a very important role in the SEP transport process. The third effect is the realistic geometry of CME and its shock. Magnetic field lines can be distorted by the CME shock, which is important for the acceleration and transport of SEPs (Zank et al. 2006). Sokolov et al. (2004) simulated particle acceleration and transport as the CME shock wave evolves with radial distance from 4 to 30 $R_\odot$ from the Sun. With a numerical solution of a fully three-dimensional MHD model, the realistic structures of CME and its shock can be derived. Their simulation results demonstrate that the diffusive shock acceleration theory can account for the increase of high-energy protons (hundreds of MeV) during solar eruptions.

In all these previous works, it was generally assumed that particles are transported only along the magnetic field lines. This assumption was justified, if, according to an early theory (Jokipii 1966), the perpendicular diffusion coefficient is generally much smaller than the parallel one. However, perpendicular diffusion coefficients change significantly from event to event. For some events, observation results show that the perpendicular diffusion coefficients could be comparable to the parallel ones (Dwyer et al. 1997; Zhang et al. 2003). This phenomenon has also been obtained by the test particle simulations that included nonlinear effects of magnetic turbulence (Qin et al. 2002a, 2002b;

Qin 2002). Later on, Matthaeus et al. (2003), Shalchi et al. (2004), Bieber et al. (2004), and Qin (2007) developed a nonlinear guiding center diffusion theory and found a better agreement with numerical simulations and observations. Furthermore, new observations from *STEREO* show that even some impulsive $^3$He-rich events (Wiedenbeck et al. 2010) can cover a much wider longitudinal extent than the width of solar flare, indicating that there is significant perpendicular particle transport.

There seems to be an agreement that SEPs can still be observed on the field lines not connected to the source through particle transport across magnetic field lines. As a result, the coverage of SEP events can be much larger than the width of particle source. In order to investigate SEPs' propagation in the heliosphere, Zhang et al. (2009) calculated the transport of SEPs in the three-dimensional Parker IMF from a source near the Sun to anywhere in the interplanetary space. Further studies have been done comparing various numerical simulations with spacecraft observations (He et al. 2011; Qin et al. 2011). The investigation in these works reveals that the perpendicular diffusion significantly influences SEP transport, especially when an observer is not connected to particle source by the IMF. However, it is noted that in these models (Zhang et al. 2009; He et al. 2011; Qin et al. 2011) the sources of SEPs are fixed near the solar surface, which is more appropriate for high-energy SEPs. On the other hand, for low-energy SEPs, the CME shock can continuously accelerate particles up to radial distances of several AU (Cane et al. 1988; Reames 1999).

In this paper, we study the effects of perpendicular diffusion on low-energy SEPs continuously produced by the interplanetary shock propagating in a three-dimensional IMF. The shock is treated as a moving source of particles, while no assumptions about acceleration mechanism are made. We investigate the time profiles of SEP flux and anisotropy as measured by an observer at 1 AU with various connections to the shock. In Section 2, we describe the SEP transport model and the shock model. In Section 3, we show our simulation results. In Section 4, we summarize our results and their implications.

## 2. MODEL

In this work we model the transport of SEPs following the same method in our previous research, (e.g., Qin et al. 2006; Zhang et al. 2009). We use a three-dimensional focus transport equation of SEPs, which can be written as (Skilling 1971; Schlickeiser 2002; Qin et al. 2006; Zhang et al. 2009)

$$\frac{\partial f}{\partial t} - \nabla\cdot(\boldsymbol{\kappa}_\perp\cdot\nabla f) + (v\mu\hat{\boldsymbol{b}} + \boldsymbol{V}^{\rm sw})\cdot\nabla f + \frac{dp}{dt}\frac{\partial f}{\partial p} + \frac{d\mu}{dt}\frac{\partial f}{\partial \mu} - \frac{\partial}{\partial\mu}\left(D_{\mu\mu}\frac{\partial f}{\partial\mu}\right) = 0, \quad (1)$$

where $f(\boldsymbol{x}, \mu, p, t)$ is the gyrophase-averaged distribution function, $\boldsymbol{x}$ is the position in a nonrotating heliographic coordinate system, $\hat{\boldsymbol{b}}$ is a unit vector along the local magnetic field, $p$ is the particle momentum in the solar wind frame, $\mu$ is the particle pitch-angle cosine in the solar wind frame, $t$ is the time, $v$ is the particle speed, and $\boldsymbol{V}^{\rm sw}$ is the solar wind velocity. The adiabatic cooling effect term, $dp/dt$, is written as (Skilling 1971; Qin et al. 2004)

$$\frac{dp}{dt} = -p\left[\frac{1-\mu^2}{2}(\nabla\cdot\boldsymbol{V}^{\rm sw} - \hat{\boldsymbol{b}}\hat{\boldsymbol{b}}:\nabla\boldsymbol{V}^{\rm sw}) + \mu^2\hat{\boldsymbol{b}}\hat{\boldsymbol{b}}:\nabla\boldsymbol{V}^{\rm sw}\right]. \quad (2)$$

The time evolution of $\mu$ is written as (Roelof 1969; Isenberg 1997; Kota & Jokipii 1995)

$$\frac{d\mu}{dt} = \frac{1-\mu^2}{2}\left[-\frac{v}{L} + \mu(\nabla\cdot\boldsymbol{V}^{\rm sw} - 3\hat{\boldsymbol{b}}\hat{\boldsymbol{b}}:\nabla\boldsymbol{V}^{\rm sw})\right], \quad (3)$$

where the magnetic focusing length $L$ is a derivative of the IMF strength $B$ $L = (\hat{\boldsymbol{b}}\cdot\nabla\ln B)^{-1}$. The relationship of the parallel mean free path (mfp) $\lambda_\parallel$ and $D_{\mu\mu}$ is written as (Jokipii 1966; Earl 1974)

$$\lambda_\parallel = \frac{3v}{8}\int_{-1}^{+1}\frac{(1-\mu^2)^2}{D_{\mu\mu}}d\mu. \quad (4)$$

The radial mean free path $\lambda_r$ is assumed to be a constant throughout heliosphere and the parallel mean free path $\lambda_\parallel$ is given by (Bieber et al. 1994)

$$\lambda_r = \lambda_\parallel\cos^2\psi, \quad (5)$$

where $\psi$ is the angle between the radial direction and the local magnetic field direction. We follow the model of pitch-angle diffusion coefficient from Beeck & Wibberenz (1986):

$$D^r_{\mu\mu} = D_{\mu\mu}/\cos^2\psi = D_0 v p^{-2/3}\{|\mu|^{q-1} + h\}(1-\mu^2), \quad (6)$$

where the constant $D_0$ is used to control the magnetic field's fluctuation level. The constant $q$ is chosen $q = 5/3$ for a Kolmogorov spectrum type of the spectral power density of magnetic field turbulence in the inertial range. The constant $h$ comes from the nonlinear effects of magnetic turbulence on pitch-angle diffusion at $\mu = 0$ (Qin & Shalchi 2009). We have chosen a relatively large value of $h = 0.2$, but it does not significantly affect the particle mean free path.

The perpendicular diffusion coefficient is assumed to be

$$\boldsymbol{\kappa}_\perp = \kappa_0\left(\frac{v}{c}\right)\left(\frac{p}{1\ {\rm GeV}c^{-1}}\right)^{2/3}\left(\frac{B_e}{B}\right)\left(\mathbf{I} - \hat{\boldsymbol{b}}\hat{\boldsymbol{b}}\right), \quad (7)$$

where $B_e$ is the magnetic field strength at the Earth and $B$ is the magnetic field strength at the location of a particle. $\mathbf{I}$ is a unit tensor. $\boldsymbol{\kappa}_\perp$ is set to be independent of $\mu$ for simplicity, because any of its $\mu$ dependence will be averaged out through a much faster pitch-angle diffusion.

The anisotropy A is defined as

$$A = \frac{3\int_{-1}^{1} f(\mu)\mu d\mu}{\int_{-1}^{1} f(\mu)d\mu}, \quad (8)$$

where $f(\mu)$ is the differential flux.

We use a partial spherical shell to model the cross-section of CME shock which is shown in Figure 1. In the figure, the shock front is indicated by the dashed arc line, and the shock nose is indicated by the dashed-arrow radial line passing through the center of the shock. The small circles, which are called cobpoints (Heras et al. 1995), indicate the locations of the shock front which are magnetically connected to the observers. As the shock propagates outward, the cobpoints move along the shock front toward the east. In our model, the shock front has a fixed solid angle. Note that the observer's field line is not connected to the shock front all the time. For example, the field line of the observer C is not connected to the shock at the beginning, but later, as the shock front moves to a larger radial distance than that of the observer, the field line becomes connected to the

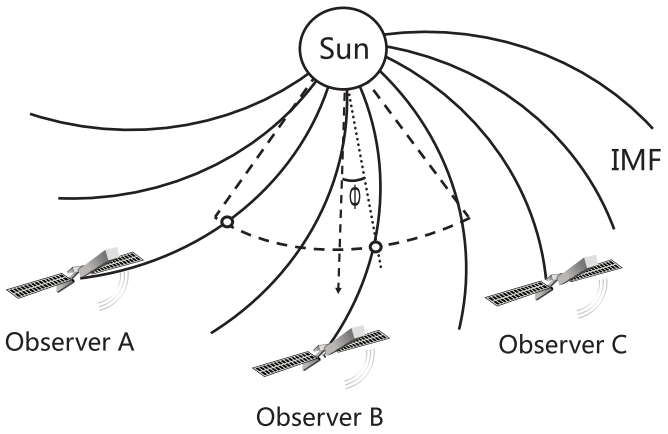


**Figure 1.** Geometry of a CME shock cross-section with three observers at different locations. The dashed-arrow radial line indicates the shock nose. The two circles represent the two cobpoints.

shock. Eventually, the observer will be disconnected from the shock as the shock continues to propagate outward.

We use boundary values to model SEP injection from the shock. The boundary condition is chosen to have the following form (Kallenrode & Wibberenz 1993, 1997; Kallenrode 2001):

$$f_b(r, \theta, \varphi, p, t) = a \cdot \delta(r - v_s t) \cdot S(r, \theta, \varphi, p) \cdot p^{-\gamma} \cdot \xi(\theta, \varphi), \quad (9)$$

where $S(r, \theta, \varphi, p)$ is the shock efficiency

$$S(r, \theta, \varphi, p) = \left(\frac{r}{r_c}\right)^{\alpha(p)} \cdot \exp\left[-\frac{|\phi(\theta, \varphi)|}{\phi_c(p)}\right], \quad (10)$$

and $\xi(\theta, \varphi)$ indicates the spatial scale of the shock front

$$\xi(\theta, \varphi) = \begin{cases} 1 & \text{if } |\phi(\theta, \varphi)| \leqslant \phi_s \\ 0 & \text{otherwise,} \end{cases} \quad (11)$$

where the shock radial distance $r = r_0 + r_s$, $r_0$ is the inner boundary, $r_c = 1$ AU, $\alpha(p)$ controls the variation of particle injection efficiency as a function of radial distance, $\phi$ is the angle between shock nose and any point at the shock front where the particles are injected, $\phi_c$ describes how fast the shock efficiency decreases toward the flanks of the shock, and $\phi_s$ is the half-angular width of the shock. Particles injected at the shock have an isotropic distribution.

We use a time-backward Markov stochastic process method to solve the transport Equation (1) (Zhang 1999). The initial boundary value problem of the SEP transport equation can be reformulated with a set of stochastic differential equations, so it can be solved by a Monte Carlo simulation of Markov stochastic process, and the SEP distribution function can be derived. In the simulation, shock is divided into a series of shells positioned at $r = r_0 + (n + 0.5)\Delta r$ in the time range $[n\Delta t, (n + 1)\Delta t)$, with $\Delta t = \Delta r / v_s$, and $n = 0, 1, 2, \ldots, n_0$. Here, we set the distance between adjacent shells $\Delta r$ small enough, i.e., $\Delta r = 3 \times 10^{-4}$ AU, to make the discrete effects of shells negligible. For every shock shell, we trace particles from the observation time back to the initial time of source particle injection. Only those particles in the source region at the initial time contribute to the statistics. For a detailed description of the method, please refer to Qin et al. (2006). In this paper, the shell model is similar to a series of onion shells which are the region swept by the shock (Zank et al. 2000). Because there is no reliable theory for the calculation of particle injection at the shock, we choose this shell model with an assumed particle injection to model the effect of particle acceleration by the CME shock. We also neglect the effect of strong scattering by enhanced waves in the vicinity of the shock. After particles are released, they will not be reaccelerated even when they encounter the shock at a later time.

**Table 1**
Model Parameters Used in the Calculations

| Parameter | Physical Meaning | Value |
|---|---|---|
| $V^{sw}$ | Solar wind speed | 400 km s$^{-1}$ |
| $v_s$ | Shock speed | 870 km s$^{-1}$ |
| $\phi_s$ | Shock width | 35° |
| $r_O$ | Observer solar distance | 1 AU |
| $\theta_O$ | Observer latitude | 90° |
| $\phi_O$ | Observer longitude | 0° |
| $\gamma$ | Injection spectrum | −5.5 |
| $E$ | Particles energy | 5 MeV |
| $\lambda_r$ | Particle radial mean free path | 0.1 AU[a] |
| $\lambda_\perp$ | Particle perpendicular mean free path | 0.0025 AU[b] |
| $r_{b0}$ | Inner boundary | 0.05 AU |
| $r_{b1}$ | Outer boundary | 50 AU |
| $r_c$ | Solar distance unit | 1 AU |

**Notes.**
[a] For 5 MeV particles throughout heliosphere.
[b] For 5 MeV particles at 1 AU.

## 3. RESULTS

The parameters used are listed in Table 1 unless otherwise stated in the text. Note that the interplanetary field is the Parker field. In addition, the ratio of the perpendicular mean free path to the parallel one at 1 AU is 0.0125. The perpendicular mean free path depends on the momentum of particle and local magnetic field strength as described in Equation (7).

### 3.1. Constant Shock Efficiency

Figure 2 shows our simulation results of the omnidirectional flux and anisotropy for 5 MeV protons in models with and without perpendicular diffusion. The left and right panels indicate the cases with and without adiabatic cooling, respectively. The shock width is 360°, and the shock efficiency $S$ is set to be a constant ($\alpha = 0, \phi_c = \infty$). The vertical dashed line indicates the moment when the shock passes the observer at 1 AU.

From Figure 2, we can see that, in all of the panels, the results with and without perpendicular diffusion are almost the same. This is because of the spherical symmetry of the SEP source. Comparing the left and right panels, we can find that the adiabatic cooling effect makes a significant difference in the time profiles of SEP fluxes. When there is no adiabatic cooling (left panels), the fluxes rise all the time. Since the shock always releases energetic particles, the number of particles in interplanetary space increases with the time. However, when there is adiabatic cooling (right panels), the fluxes decrease after the shock passage of the observer. Because of the adiabatic cooling effect, the observed particles at 1 AU have less energies than when they were injected at the source. Since the SEP source has a negative energy spectral index, lower flux would be observed for particles at the same energy at a later time.

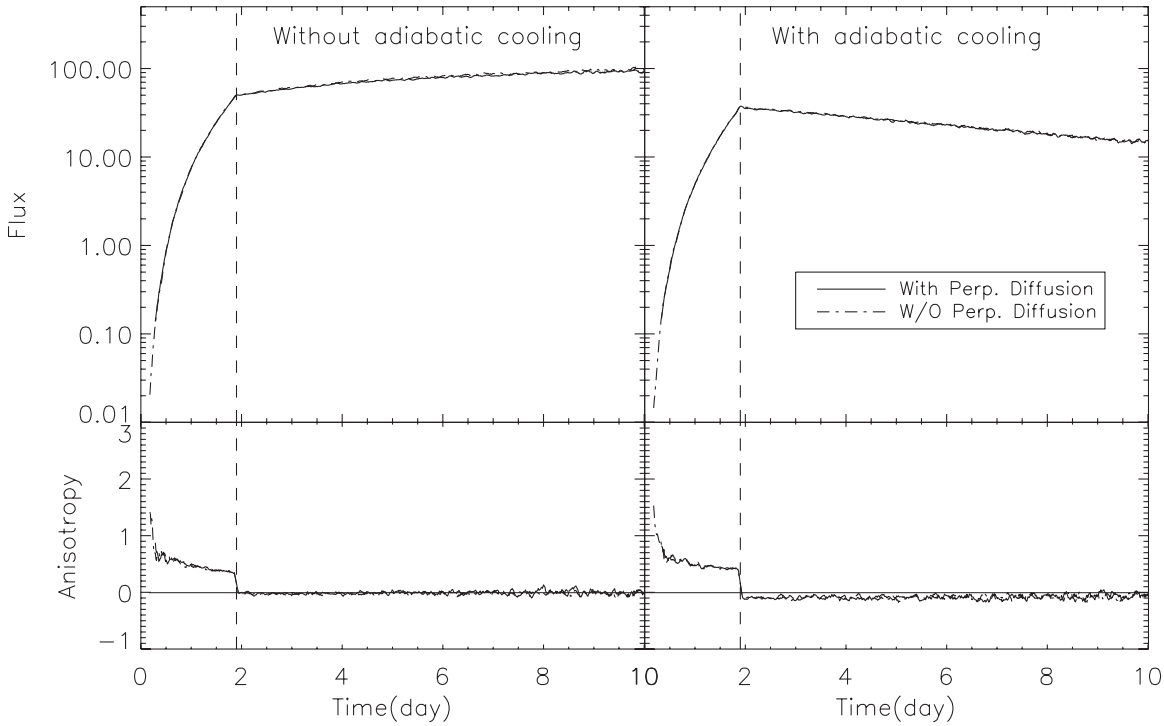


**Figure 2.** Comparison of 5 MeV protons flux and anisotropy with perpendicular diffusion (solid line) and without perpendicular diffusion (dash-dotted line). The left and right panels show the results without and with adiabatic cooling effects, respectively. The shock width is 360° and the shock efficiency is a constant. The vertical dashed line indicates the moment when the shock passes the observer at 1 AU in each panel.

It is also interesting to study the anisotropy of particle flux. Before the shock reaches the observer, particles are released from the shock at distances $r < 1$ AU so that the anisotropy is always positive. At the shock passage of the observer, the anisotropy suddenly jumps to zero, because the injected energetic particles are set to be isotropic in the source region. After the passage of the shock, the anisotropy with and without adiabatic cooling behaves differently. Without the adiabatic cooling effect, the anisotropy remains near zero. However, with the adiabatic cooling effect, the anisotropy keeps a small negative value. Generally, the particles originating from injections at $r < 1$ AU have experienced more adiabatic energy loss, so their contribution to the observed particle flux is smaller than those originating from injections at $r > 1$ AU. As a result, the anisotropy has a negative value. Since the adiabatic cooling is an important effect, we include it in all of the following simulations.

Figure 3 shows the simulation results with shock efficiency $S$ as a constant ($\alpha = 0, \phi_c = \infty$). The observer is located at 1 AU equator and 0° longitude. The propagation direction of the shock is indicated by the direction of shock nose. In the top six panels, all of the shock noses are located in the equatorial plane, but point to different longitudes. The labels E20, CM (center meridian), and W20 indicate that the shock nose points to 20° east, 0°, and 20° west, respectively, all relative to the observer. In the last two panels, all of the longitudes of the shock noses are set at 0°, but their latitudes are different, i.e., 20° north (N20) and 40° north (N40) from the equator. The shock nose directions relative to the observer are similarly named in the rest of the paper. The vertical dashed line indicates the moment of the shock passage of 1 AU, but it does not ensure the shocks pass the observer because of the limited size of shock width. In the following, if the shock actually passes the observer at 1 AU, the case is recorded as "the shock passage of the observer," otherwise it is recorded as "the shock passage of 1 AU." The time interval between the two short vertical solid lines indicates the time period during which the observer is connected to the shock by the IMF. Note that since the enhanced turbulence and local particle acceleration at the shock are not included in the model, a spike in the particle flux is absent at the shock passage of the observer.

Figures 3(a) and (b) show the results for events W70 and W40, respectively. We can refer to these events as the western events. In the beginning, there is no obvious difference with and without perpendicular diffusion, because the observer's field line is connected to the shock since the onset time in each event. The shock is not detected by the observer when passing 1 AU. After the observer's field line is disconnected from the shock, the flux starts to decay. However, the flux decays more slowly with perpendicular diffusion, because after the shock is disconnected from the field line, "new" particles can be continuously injected into the observer's field line through perpendicular diffusion. In addition, the anisotropy is larger than zero at the beginning, and then gradually decreases to zero as the shock propagates outward. During the entire event, the time profiles of SEP anisotropy are almost the same with and without perpendicular diffusion.

Figures 3(c), (d), and (e) show results for events W20, CM, and E20, respectively. We can approximately refer these events as center meridional (CM) events. For the CM events, the observer's field line is not connected to the shock at the onset time. With perpendicular diffusion, the SEP event starts earlier. In each event, the peak of flux appears at the shock passage of the observer. After the observer's field line is disconnected from the shock, the flux decays more quickly without perpendicular diffusion.

Figure 3(f) shows the results for the event E40 which is referred to as the eastern event. Note that the observer's field

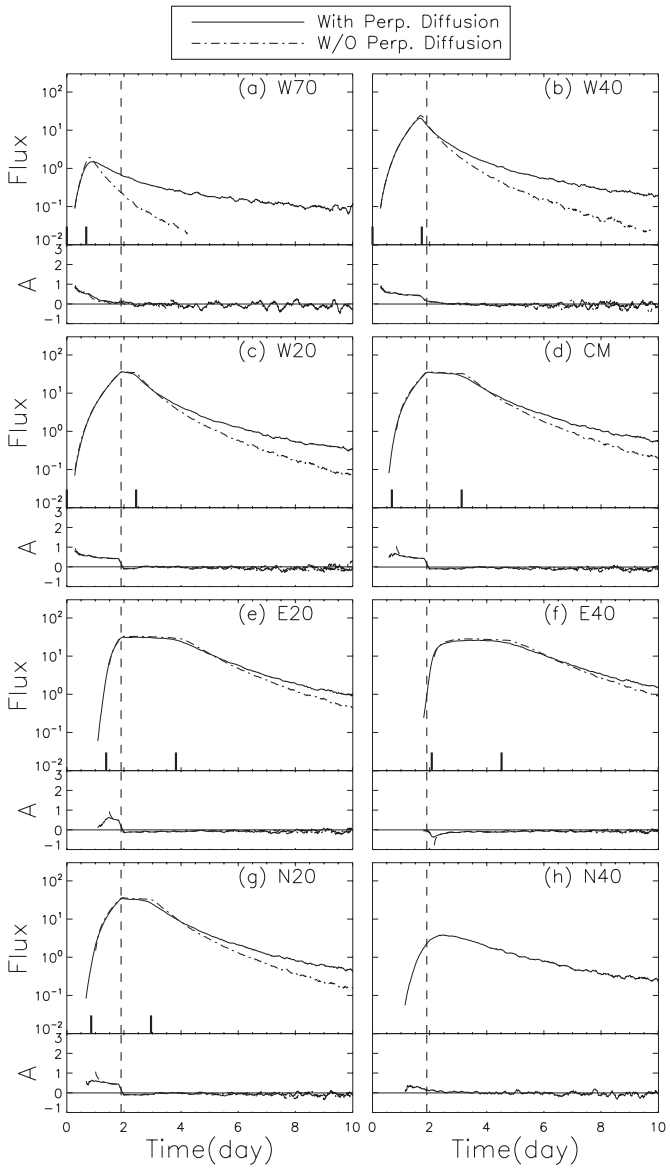


**Figure 3.** Comparison of 5 MeV protons flux and anisotropy with perpendicular diffusion (solid lines) and without perpendicular diffusion (dash-dotted lines). The shock width is 70° and the shock efficiency is a constant. The vertical dashed line indicates the moment of the shock passage. The time interval between the two short vertical solid lines indicates the time during which the observer's field line is connected to the shock. Different sub-figure indicates different shock nose directions relative to the observer.

line is not connected to the shock until the shock passage of 1 AU. Without perpendicular diffusion, the anisotropy is significantly less than zero at the beginning, which means most of the particles are moving toward the Sun at that time. However, with perpendicular diffusion, the observed particles are nearly isotropic.

Figure 3(g) shows the results for the event N20, in which the SEP flux and anisotropy have behaviors similar to those in the CM events, i.e., the flux peak appears at the shock passage of the observer. In the event N40 shown in Figure 3(h), the time profiles of flux and anisotropy behave differently from that in the event N20. In the event N40, the observer's field line is not connected to the shock at all times, so the observer can only detect the particles coming through the perpendicular diffusion. The anisotropy is always approximately equal to zero, and the flux peak appears after the shock passage of 1 AU.

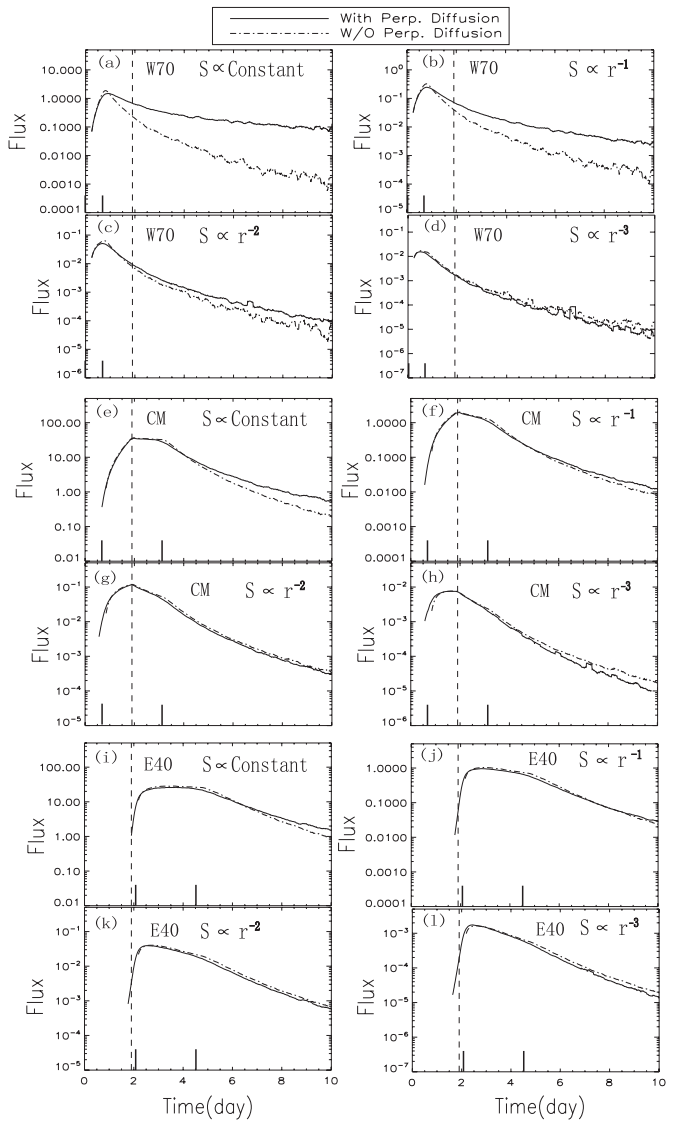


**Figure 4.** Comparison of 5 MeV proton fluxes in the cases of different power indices of shock efficiency.

### *3.2. Variable Shock Efficiency*

Figure 4 shows the fluxes of 5 MeV protons with different source efficiency power indices (0, −1, −2, and −3), which controls how fast the shock efficiency changes as a power-law function of the radial distance.

In panels (a)–(d) of Figure 4, the shocks are in the direction of W70. It is shown that in Figure 4(a), when the source efficiency is a constant, the flux decreases more slowly with perpendicular diffusion. As the shock efficiency decreasing in panels from (a) to (c), the fluxes with perpendicular diffusion decrease more and more quickly, and the difference in fluxes between the cases with and without perpendicular diffusion becomes smaller and smaller. Especially in Figure 4(d), when the index is −3, the flux with perpendicular diffusion becomes even smaller than that without perpendicular diffusion. It is known that with perpendicular diffusion two kinds of processes are in operation: the gain of particles arriving at the observer's field line from nearby field lines and the loss of particles from the observer's field line. The gain (or loss) of particles with perpendicular diffusion can make the flux decrease more slowly (or quickly) in the decay phase than without

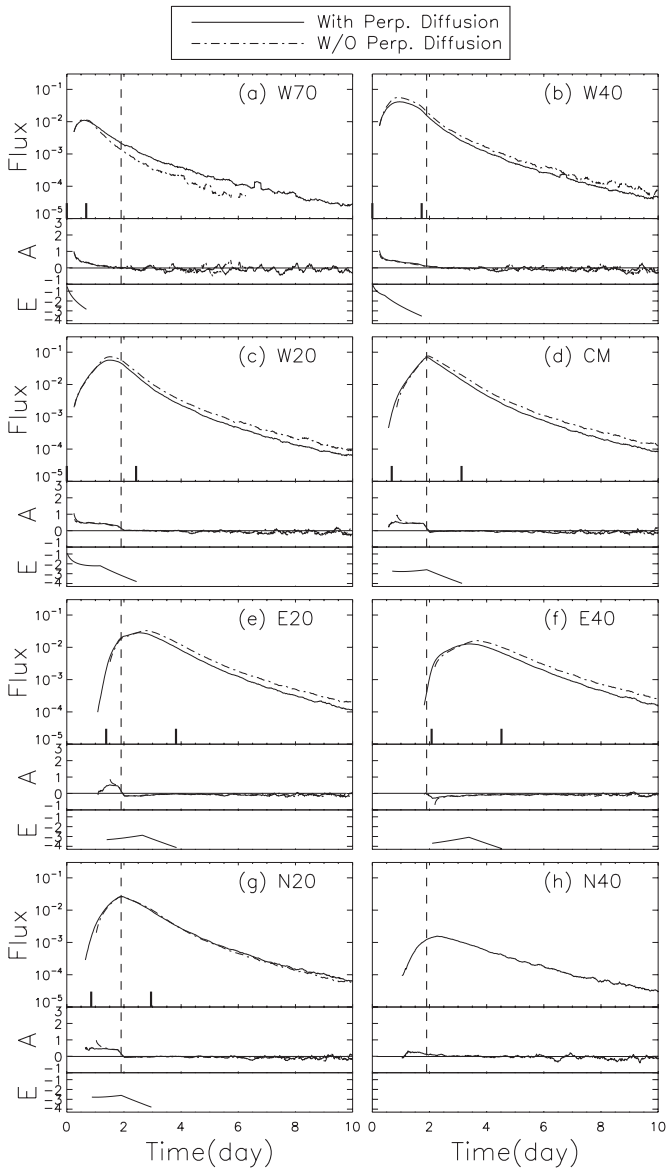


**Figure 5.** Same as Figure 3 except that the shocks' efficiency changes with a power law in radial distance and an exponential law in angle distance from the shock nose, $S \sim (r/r_c)^{-2} \exp(-|\phi|/15^\circ)$, and that an additional panel showing the time profile of cobpoint efficiency $E = \log(S)$ is added for each sub-figure.

perpendicular diffusion. In addition, the power index of the shock efficiency mainly influences the gains of particles. As the shock efficiency power index decreases from 0 to −3, particles arriving at the observation point by crossing field lines at a later time become less important. In Figure 4(d), the gain of particles is too slow to compensate for the loss of particles, so the flux without perpendicular diffusion is larger than that with perpendicular diffusion. In panels (e)–(h) of Figure 4 the shocks propagate in the CM direction, and in panels (i)–(l) of Figure 4 the shocks head toward E40. Compared with the case of W70, we can see a similar behavior in the decay phases of fluxes in the cases of CM and E40.

Figure 5 shows the results of simulations similar to that shown in Figure 3. The only difference is that now the shock efficiency $S$ changes as a power-law function of the radial distance times an exponential function of the angle distance from the shock nose, $S \sim (r/r_c)^{-2} \exp(-|\phi|/15^\circ)$. In addition, the $y$-title "E" in each panel shows the time evolution of the shock's logarithm efficiency at the cobpoint ($E \equiv \log S$). Although the flux is not just affected by strength of boundary condition at the current time, the cobpoint efficiency is still very important, because the speed of particles is much faster than that of shock and the parallel diffusion coefficient is larger than the perpendicular one.

In the events W70 and W40 shown in Figures 5(a) and (b), respectively, the shock efficiency at the cobpoint decreases with time very quickly, so the peaks of fluxes appear earlier than in the cases with a constant shock efficiency (Figures 3(a) and (b)). In the event W70, the observer's field line is disconnected from the shock very early, so there are only a small number of particles arriving at the observation point directly from the source following the field lines. With perpendicular diffusion, the flux decreases more slowly than that without perpendicular diffusion. However, in the event W40 shown in Figure 5(b), after the observer's field line is disconnected from the shock, the flux decays more quickly with perpendicular diffusion than without it. Since the observer's field line is connected to the shock for a longer time than that in the event W70, more particles arrive at the observation point directly from the shock along the field line, but with perpendicular diffusion, the loss of particles in the event W40 is faster than the gain of particles. Therefore, the flux decreases more quickly with perpendicular diffusion than without it. Since the observer's field line is disconnected from the shock before the shock passage of 1 AU, the anisotropy gradually decreases to zero, and there is no jump at the shock passage in these events.

In the events W20, CM, E20, and E40 shown in Figures 5(c), (d), (e), and (f), respectively, when the cobpoint reaches the shock nose, the shock efficiency reaches the maximum, and the peak of flux appears in each event. After that, the fluxes gradually decay with the time. In particular, for the event CM in Figure 5(d), the cobpoint reaches the shock nose at 1 AU, so the peak of flux appears at the shock passage of the observer. However, for the event W20 in Figure 5(c), since the cobpoint reaches shock nose inside 1 AU, the peak of flux appears before the shock passage of the observer. Likewise, for the events E20 and E40 in Figures 5(e) and (f), respectively, the flux peaks appear after the shocks passage for similar reasons. In the event N20 shown in Figure 5(g), the flux and anisotropy behave similarly to those shown in the event CM. However, for the event N40 shown in Figure 5(h), the observer's field line is not connected to the shock the entire time and the cobpoint does not exist anymore, so the observer can only detect the particles coming through perpendicular diffusion.

Figure 6 shows the simulations of 5 MeV proton with different perpendicular diffusion coefficients. The perpendicular mean free path is set to $\lambda_\perp = 0.0025$ AU and $\lambda_\perp = 0.025$ AU, where radial mean free path is $\lambda_r = 0.1$ AU ($\lambda_\parallel \approx 0.2$ AU at 1 AU). With the larger perpendicular mean free path, the onset time of flux moves to an earlier time. In each of the E20 and E40 events, the peak time of flux comes earlier with stronger perpendicular diffusion. Furthermore, with stronger perpendicular diffusion, the peak intensity of flux is less than that with weaker perpendicular diffusion in all the events, except the N40 event. In the N40 event, all the particles arrive at the observation point by crossing field lines, so the flux should be larger with stronger perpendicular diffusion. Anisotropy in the N40 event is always near zero. It is also noted that there is no significant difference in the anisotropy with different perpendicular diffusion coefficients in all the events shown in this figure.

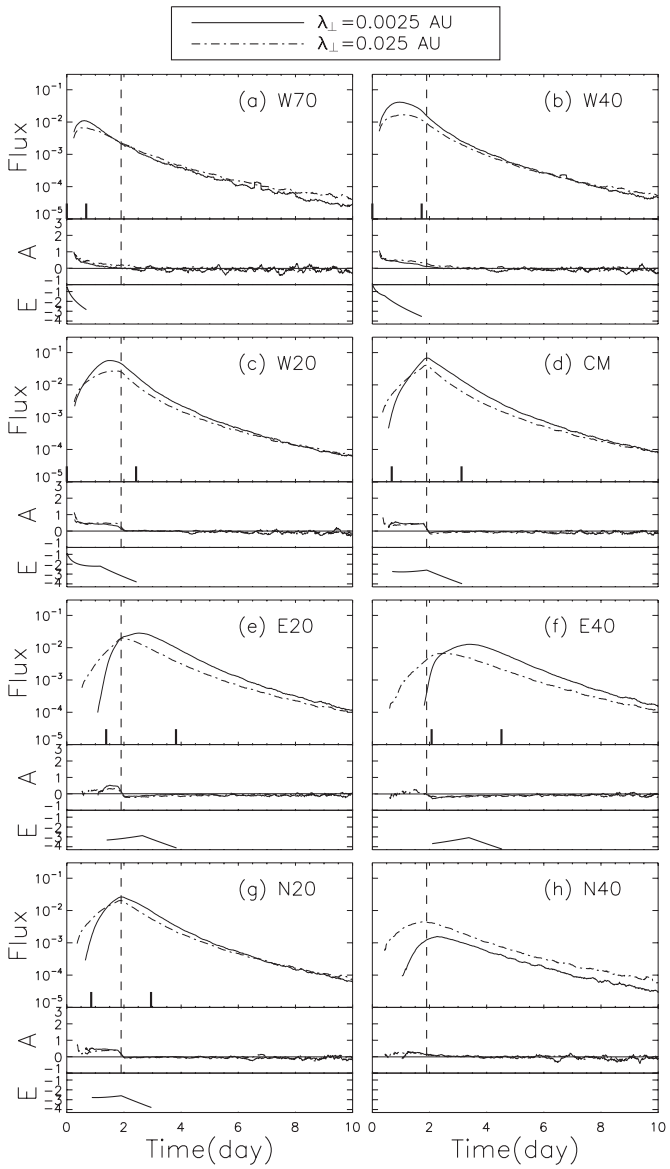


**Figure 6.** Same as Figure 5 except that different line styles indicate different perpendicular mean free paths.

## 4. SUMMARY

In our model, we assume the ICME shock as a moving source of SEPs with varying strength as a function of location and time, as it propagates through the Parker IMF. We investigate how the injected particles transport with varying conditions of shock geometry and mean free paths. Our SEP transport equation essentially includes all necessary particle transport mechanisms, such as particle streaming along field line, magnetic focusing in the diverging IMF, adiabatic deceleration in the expanding solar wind, and the diffusion parallel and perpendicular to the IMF. However, comparing with previous works (e.g., Zank et al. 2000; Ng et al. 2003; Sokolov et al. 2004), we neglected a few mechanisms, for example, particle acceleration by the CME shock, wave generation by the streaming particles, and realistic geometry of the CME shock. Since the prediction of SEP flux requires a precise mechanism for particle injection into the diffusive shock acceleration, which is currently not available, we have adopted a diffusion model to describe some general effects of particle transport processes. In this paper, we have studied the effects of perpendicular diffusion on 5 MeV protons produced by the ICME shock by numerically solving the focused Fokker–Planck transport equation of energetic particles. We have shown the time profiles of particle flux and anisotropy as observed at 1 AU in the cases with and without perpendicular diffusion. Our new findings are listed as follows.

1. Adiabatic cooling plays an important role in the transport of SEPs. Adiabatic cooling can cause SEPs to become less energetic while transporting in the heliosphere, so that the SEPs with the same energy observed later generally originate with higher energies at the source. Because the source has a negative energy spectral index, the flux decreases more quickly with adiabatic cooling than without it. The SEP flux decay rate and anisotropy are affected by the adiabatic cooling effect and the spectral index of the source particles.
2. With perpendicular diffusion, particles can be detected before the observer is connected to the shock by field lines, and the particles detected at the onset time have experienced significant perpendicular diffusion. Therefore, the anisotropy is smaller with perpendicular diffusion at the onset than without it. Since the SEP source is assumed isotropic and particles can cross the shock freely in our model, the anisotropy can jump to zero or even a negative value at the shock passage of the observer. No obvious difference is seen in the anisotropy with and without perpendicular diffusion, except in the onset time of field line connection to the shock.
3. With perpendicular diffusion, two kinds of processes are in operation, the gain of particles from other field lines to the observer's field line, and the loss of particles by leaving the observer's field line. The gains (or losses) of particles can make the flux decrease more slowly (or quickly) in the decay phase than without the perpendicular diffusion.
4. When the shock efficiency is a constant, the time profile of SEP flux is significantly influenced by the shock position. After the observer's field line is disconnected from the shock, the flux begins to decay with the time. With perpendicular diffusion, the gain of particles is faster than the loss of particles, so the flux decreases more slowly than without it.
5. When the shock efficiency changes with a power-law function of the radial distance, the time profile of SEP flux is influenced by both the shock efficiency and shock position. When the shock efficiency is a constant, the flux decreases more slowly with perpendicular diffusion than without it. However, as the shock efficiency decreases, the loss of particles becomes increasingly significant relative to the gain, and the difference in the fluxes with and without perpendicular diffusion gets smaller. Especially, when the power index is small enough, a quick decrease of the shock efficiency can make the flux decrease more quickly with perpendicular diffusion.
6. When the shock efficiency varies with a power-law function of the radial distance and an exponential law in the angular distance from the shock nose, $S \sim (r/r_c)^{-2} \exp(-|\phi|/15^\circ)$, the flux peaks when the cobpoint reaches the shock nose. In addition, with a larger perpendicular mean free path, the onset time of flux is earlier, and the peak intensity is lower, except for the case in which the observer's field line is not connected to the shock for the entire time. In the case that has no direct connection to the shock, all particles reach the observation point by crossing the field lines, so the peak

intensity is higher with a larger perpendicular mean free path.

In future works, we will extend our model to studying particle acceleration by CME shocks. We intend to include a realistic three-dimensional CME shock, local wave generated by streaming particles, and diffusion coefficients derived from some advanced theories of particle transport (e.g., NLGC theory; Matthaeus et al. 2003). In this way, more physical mechanisms in the gradual SEP events can be studied.

The authors thank the anonymous referee for valuable comments. This research work was partly supported by grants NNSFC 41125016, NNSFC 40921063, NNSFC 41074125, CMA grant GYHY201106011, and the National High-tech R&D Program of China (863 Program) 2010AA122200. The computations were performed by the Numerical Forecast Modeling R&D and VR System of the State Key Laboratory of Space Weather and Special HPC work stand of the Chinese Meridian Project. M.Z. was supported in part by NASA Grants NNX08AP91G, NNX09AG29G, and NNX09AB24G.

## REFERENCES

Beeck, J., & Wibberenz, G. 1986, ApJ, 311, 437
Bieber, J. W., Matthaeus, W. H., Shalchi, A., & Qin, G. 2004, Geophys. Res. Lett., 31, L10805
Bieber, J. W., Matthaeus, W. H., Smith, C. W., et al. 1994, ApJ, 420, 294
Cane, H. V., Reames, D. V., & von Rosenvinge, T. T. 1988, J. Geophys. Res., 93, 9555
Dwyer, J. R., Mason, G. M., Mazur, J. E., et al. 1997, ApJ, 490, L115
Earl, J. A. 1974, ApJ, 193, 231
Gordon, B. E., Lee, M. A., Möbius, E., & Trattner, K. J. 1999, J. Geophys. Res., 104, 28263
He, H.-Q., Qin, G., & Zhang, M. 2011, ApJ, 734, 74
Heras, A. M., Sanahuja, B., Lario, D., et al. 1995, ApJ, 445, 497
Heras, A. M., Sanahuja, B., Smith, Z. K., Detman, T., & Dryer, M. 1992, ApJ, 391, 359
Isenberg, P. A. 1997, J. Geophys. Res., 102, 4719
Jokipii, J. R. 1966, ApJ, 146, 480
Kallenrode, M. 2001, J. Geophys. Res., 106, 24989
Kallenrode, M., & Wibberenz, G. 1993, in Proc. Int. Cosmic Ray Conf., 3, Proceedings of the 23rd International Cosmic Ray Conference, ed. D. A. Leahy, R. B. Hickws, & D. Venkatesan (Singapore: World Scientific), 298
Kallenrode, M., & Wibberenz, G. 1997, J. Geophys. Res., 102, 22311
Kota, J., & Jokipii, J. R. 1995, Science, 268, 1024
Lario, D., Sanahuja, B., & Heras, A. M. 1998, ApJ, 509, 415
Lee, M. A. 1983, J. Geophys. Res., 88, 6109
Lee, M. A. 2005, ApJS, 158, 38
Li, G., Zank, G. P., & Rice, W. K. M. 2003, J. Geophys. Res., 108, 1082
Liu, Y., Luhmann, J. G., Bale, S. D., & Lin, R. P. 2011, ApJ, 734, 84
Matthaeus, W. H., Qin, G., Bieber, J. W., & Zank, G. P. 2003, ApJ, 590, L53
Ng, C., Reames, D., & Tylka, A. 1999, Geophys. Res. Lett., 26, 2145
Ng, C., Reames, D., & Tylka, A. 2001, in Proc. Int. Cosmic Ray Conf., 8, Proceedings of the 27th International Cosmic Ray Conference, ed. W. Droege, H. Kunow, & M. Scholer, 3140
Ng, C., Reames, D., & Tylka, A. 2003, ApJ, 591, 461
Qin, G. 2002, PhD thesis, Univ. Delaware
Qin, G. 2007, ApJ, 656, 217
Qin, G., He, H.-Q., & Zhang, M. 2011, ApJ, 738, 28
Qin, G., Matthaeus, W. H., & Bieber, J. W. 2002a, Geophys. Res. Lett., 29, 1048
Qin, G., Matthaeus, W. H., & Bieber, J. W. 2002b, ApJ, 578, L117
Qin, G., & Shalchi, A. 2009, ApJ, 707, 61
Qin, G., Zhang, M., & Dwyer, J. R. 2006, J. Geophys. Res., 111, 8101
Qin, G., Zhang, M., Dwyer, J. R., & Rassoul, H. K. 2004, ApJ, 609, 1076
Reames, D. V. 1999, Space Sci. Rev., 90, 413
Rice, W. K. M., Zank, G. P., & Li, G. 2003, J. Geophys. Res., 108, 1369
Roelof, E. C. 1969, in Lectures in High-Energy Astrophysics, ed. H. Ögelman & J. R. Wayland (NASA SP-199; Washington, DC: NASA), 111
Schlickeiser, R. (ed.) 2002, Cosmic Ray Astrophysics (Berlin: Springer)
Shalchi, A., Bieber, J. W., Matthaeus, W. H., & Qin, G. 2004, ApJ, 616, 617
Skilling, J. 1971, ApJ, 170, 265
Sokolov, I., Roussev, I., Gombosi, T., et al. 2004, ApJ, 616, L171
Wiedenbeck, M. E., Mason, G. M., Gómez-Herrero, R., et al. 2010, in AIP Conf. Proc. 1216, Twelfth International Solar Wind Conference, ed. M. Maksimovic, N. Meyer-Vernet, M. Moncuquet, & F. Pantellini (Melville, NY: AIP), 621
Zank, G., Li, G., Florinski, V., et al. 2006, J. Geophys. Res., 111, A06108
Zank, G. P., Rice, W. K. M., & Wu, C. C. 2000, J. Geophys. Res., 105, 25079
Zhang, M. 1999, ApJ, 513, 409
Zhang, M., Jokipii, J. R., & McKibben, R. B. 2003, ApJ, 595, 493
Zhang, M., Qin, G., & Rassoul, H. 2009, ApJ, 692, 109